J Nanopart Res (2017) 19: 243
DOI 10.1007/s11051-017-3940-5

RESEARCH PAPER

Controllable synthesis of $FeVO_4$@TiO_2 nanostructures as anode for lithium ion battery

H. Zheng · Y. Yang · X. Liu · Z. Guo · C. Feng

Received: 12 April 2017 / Accepted: 26 June 2017 / Published online: 12 July 2017

Abstract $FeVO_4$@TiO_2 nanocomposite was fabricated via a simple and cost-effective approach. The $FeVO_4$ nanorods were synthesized by a hydrothermal method combined with calcination route without using any template and then coated with TiO_2 through an annealing process of dihydroxybis titanium. The $FeVO_4$ nanocomposite has a significantly enhanced electrochemical performance by coating with TiO_2. The $FeVO_4$@TiO_2 delivered a specific capacity of 1147 mAh g^{-1}, the discharge capacity remaining at 596 mAh g^{-1} after 100 cycles (at 200 mA g^{-1}), which is higher than that of pure $FeVO_4$. The discharge capacity of $FeVO_4$@TiO_2 could be as high as 337 mAh g^{-1} (at a high load current density of 10,000 mA g^{-1}). Compared with pure $FeVO_4$, $FeVO_4$@TiO_2 shows a better rate performance. The amorphous TiO_2 coating on a layer of $FeVO_4$ created efficient improved stability of the structure during the charge/discharge process. The excellent rate capability and cyclic stability of the sample proved that $FeVO_4$@TiO_2 could be used as a new anode for lithium ion battery application. The synthesis method can also be applied to synthesize other related materials with typical morphologies and properties.

H. Zheng · Y. Yang · X. Liu · Z. Guo · C. Feng (✉)
Hubei Collaborative Innovation Center for Advanced Organic Chemical Materials, Hubei University, Wuhan 430062, China
e-mail: cfeng@hubu.edu.cn

H. Zheng
Key Laboratory of Functional Materials and Chemistry for Performance and Resources of the Guizhou Education Department, Anshun University, Anshun 561000, China

Keywords $FeVO_4$ · Surface modification · Anode material · Electrochemical properties · Energy storage

Introduction

In modern times, rechargeable Li-ion batteries (LIBs) have been universally used in plug-in electric vehicles and portable electronics owing to the advantages of its high-energy density and long life (Cheng and Chen 2011). As the traditional commercial anode material, graphite with the low theoretical capacity (372 mAh g^{-1}) cannot meet the gradually increasing requirement for energy in modern times (Sun et al. 2013; Peng et al. 2005). Thus, novel anode materials with a much higher reversible capacity should be developed.

Recently, transitional metal vanadates showing the advantages of high theoretical capacity and rate performance based on the unique conversion mechanism have attracted much attention as electrode materials (Wang and Cao 2008; Huang et al. 2010; Yang et al. 2016; Lei et al. 2007; Pan et al. 2011). A wide variety of transition metal vanadates (such as $FeVO_4$, ZnV_2O_4, $Zn_3V_2O_8$, ZnV_2O_6, MoV_2O_8, CuV_2O_6, CoV_2O_6, and $Ag_2V_4O_{11}$) has been fabricated and their electrochemical performance was studied (Xi and Ye 2010; Zhu et al. 2013; Sun et al. 2011; Shi et al. 2011; Li et al. 2013; Wang et al. 2014; Zhang et al. 2015; Liang et al. 2015; Wang et al. 2012; Xiao et al. 2009). For example, Yang et al. (2014) have prepared $Co_3V_2O_8$ nanosheets, which showed excellent electrochemical performance. Ni et al. (2014) firstly reported synthesized Li_3VO_4 through hydrothermal and

annealed route method. The Li_3VO_4 delivered a good initial discharge, 396 mAh g^{-1} at a rate of 0.25 C after 100 cycles. Gan and workers (2014) synthesized hexagonal $Zn_3V_2O_8$ nanosheets, which displayed an excellent reversible capacity of 1103 mAh g^{-1}. The non-spherical structures $Co_3V_2O_8{\cdot}nH_2O$ exhibited impressive electrochemical properties with superior lithium storage capability (after 255 cycles, maintaining 847 mAh g^{-1}) (Wu et al. 2015). Yin et al. (2016) have first reported MoV_2O_8 nanorods were evaluated as an anode material and showed excellent performance.

Among transition metal vanadates, $FeVO_4$ (iron vanadate), as a promising host for anode materials, has prominent advantages due to its layered structure (short intercalated Li^+ ion distance) (Ma et al. 2011). Some reports have reported high specific capacities of the vanadates (1300 mAh g^{-1} for $FeVO_4$). Yan et al. (2016) reported the synthesis of $FeVO_4$ via a facile hydrothermal-sintering method. The $FeVO_4$ nanoparticles show initial capacities of 527 mAh g^{-1}, maintaining 430 mAh g^{-1} (after 100 cycles). A number of reports on two-dimensional (2D) nanostructure materials used to develop high performance are attributed to a large contact area and prompt Li^+ diffusion paths. Sim et al. (2012) reported amorphous $FeVO_4$ nanosheet arrays by a CVD method. The $FeVO_4$ nanosheet arrays presented high specific capacities. Liu and coworkers (2017) reported $FeVO_4$/graphene nanocomposites were synthesized via a hydrothermal and heat-treatment method. The $FeVO_4$/graphene nanocomposites delivered a good specific capacity, 1046 mAh g^{-1} after 100 cycles. An abundance of anode materials with graphene oxide nanocomposite and carbon coating composite with outstanding electrochemical performance has been reported. Titanium dioxide (TiO_2) with a protective layer is ideal for modified material, which is widely used to improve cyclic stability for the cathode material. Compared with anode materials, a few works have been conducted on anode materials coated with TiO_2. Chen et al. (2015) synthesized porous cubic Mn_2O_3@TiO_2 through precipitation-calcination route. The porous cubic Mn_2O_3@TiO_2 delivered a superior specific capacity of 936 mAh g^{-1} at a rate of 200 mA g^{-1} after 100 cycles. The highly stable TiO_2 provides protection for Mn_2O_3 from structural destruction due to the volume change during charge/discharge processes, and a new scheme is provided to solve the problem on capacity loss for transition metal oxides.

In this work, we reported the synthesis of nanostructures of $FeVO_4$ nanorods without any additives and template under hydrothermal conditions followed by calcination, using ammonium lactate titanium (IV) as modified material. The synthesis method is simple and cost effective. Compared with pure $FeVO_4$, $FeVO_4$@TiO_2 shows better electrochemical performance. The amorphous TiO_2 coating layer on $FeVO_4$ created an improvement in the stability of the structure, rate capability, and cyclic stability through the charge/discharge process. $FeVO_4$@TiO_2 synthesized by a suitable method could be used as a promising anode material for lithium-ion battery application.

Experimental

Synthesis and characterization of the samples

In the experiment, all of the chemicals were of analytical grade. One millimole of $FeCl_3{\cdot}6H_2O$ and 1 mmol NH_4VO_3 were added into 10 ml of deionized water at room temperature and stirred for 20 min, respectively. In the stirring, the NH_4VO_3 solution was added dropwise into the $FeCl_3$ solution, and after 0.5 h, the mixed solution into a 50-ml autoclave and heated at 180 °C for 2 h. The expected samples were cleaned with H_2O and ethanol, dried at 80 °C for 8 h, and calcined at 500 °C for 2 h. The $FeVO_4$ nanorods were obtained.

0.2 g of the $FeVO_4$ nanorods was added into 10 ml of NaOH solution (0.1 mmol) under stirring for 90 min, then 100 μl of ammonium lactate titanium (IV) was added under stirring for 180 min. The followed steps for synthesis of $FeVO_4$ were the same as those described above. The $FeVO_4$@TiO_2 nanostructures were obtained.

X-ray diffraction (XRD) was characterized using Cu K_α radiation by Bruker AXS (D8 diffractometer). The sizes of the samples were detected by SEM (JEOLJSM-7400F, Japan), X-ray (EDX) detector (Oxford Instruments, INCA), and TEM/HRTEM (Tecnai G2 F30, FEI company). X-ray photoelectronic spectrometer (XPS, VGESCA-LABMK II) was used to determine the valence states of the elements in the metal oxide.

Electrochemical measurements

The electrodes were prepared by pressing a mixture of polytetrafluoroethylene (PTFE) (10%), acetylene black (20%), and active material (70%) onto a nickel net. The electrodes were dried at 110 °C in a vacuum drying oven

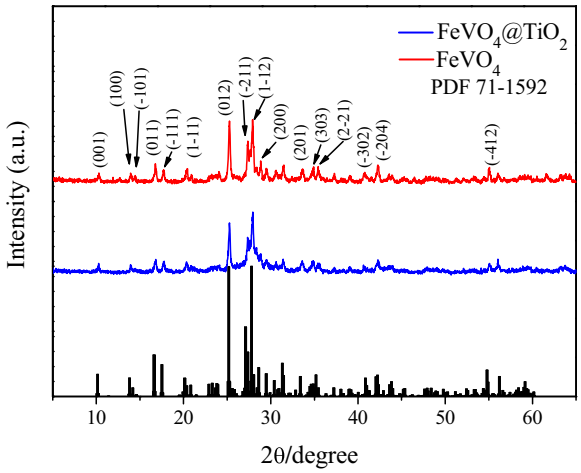

Fig. 1 XRD patterns of the $FeVO_4$ and $FeVO_4$@TiO_2 samples

for 12 h. Electrochemical experiments were performed using CR2032-type cells with Li foil as the counter electrode and composite electrodes of expected compounds. The typical mass of active material was about 1.0–1.2 mg cm^{-2}. The electrolyte was a solution of 1 M $LiPF_6$ in diethyl carbonate (DEC) and ethylene carbonate (EC) (1:1 by volume). The battery was assembled in a glove box filled with argon gas. The voltage range of 0.01 to 3.00 V and different current densities were controlled during battery tests. The cyclic voltammetry (CV) and electrochemical impedance spectroscopy (EIS) experiments were conducted by a CHI 660A electrochemical workstation.

Results and discussion

Both $FeVO_4$ nanorods and $FeVO_4$@TiO_2 nanoparticles were characterized by XRD analysis, as presented in Fig. 1. The XRD indicated that the two samples had the same single-phase structure, and the diffraction peaks of two samples are in agreement with the ordered triclinic $FeVO_4$ structure (JCPDS No. 071-1592), without any impurity phase. There are no TiO_2 diffraction peaks in

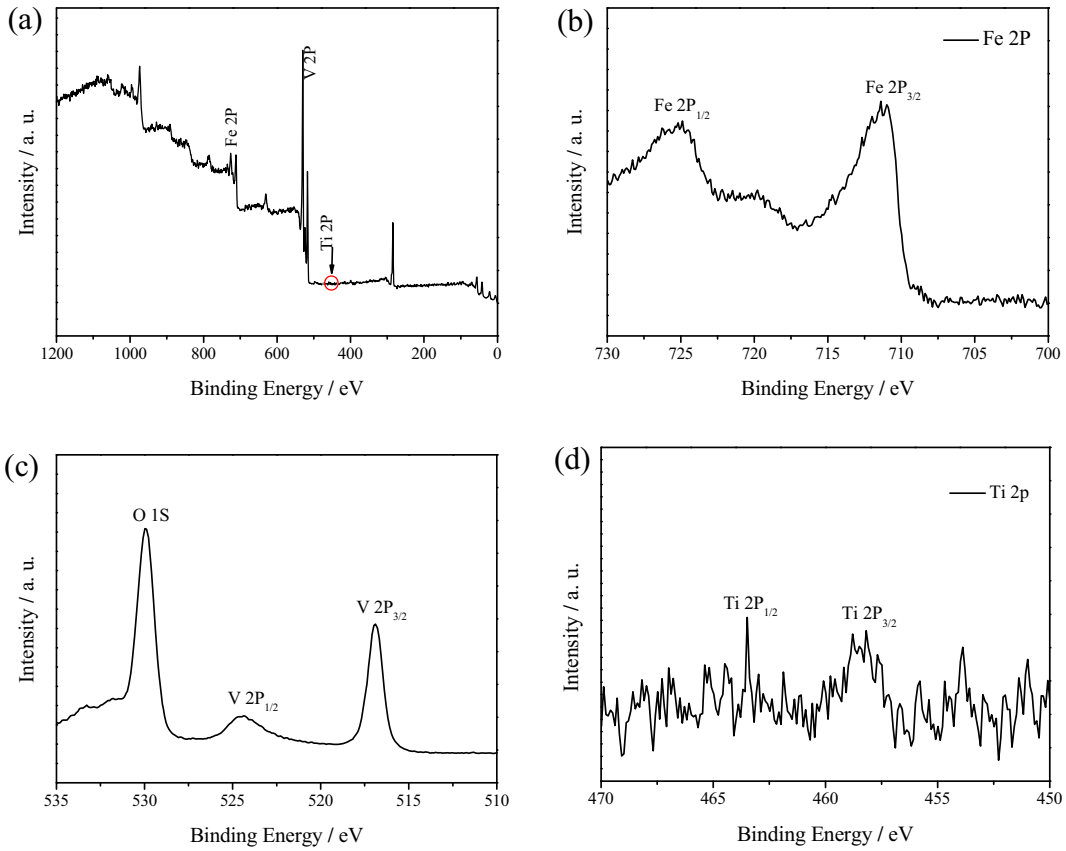

Fig. 2 XPS spectrum of **a** $FeVO_4$@TiO_2, **b** Fe2p, **c** V2p and O1S, and **d** Ti2p

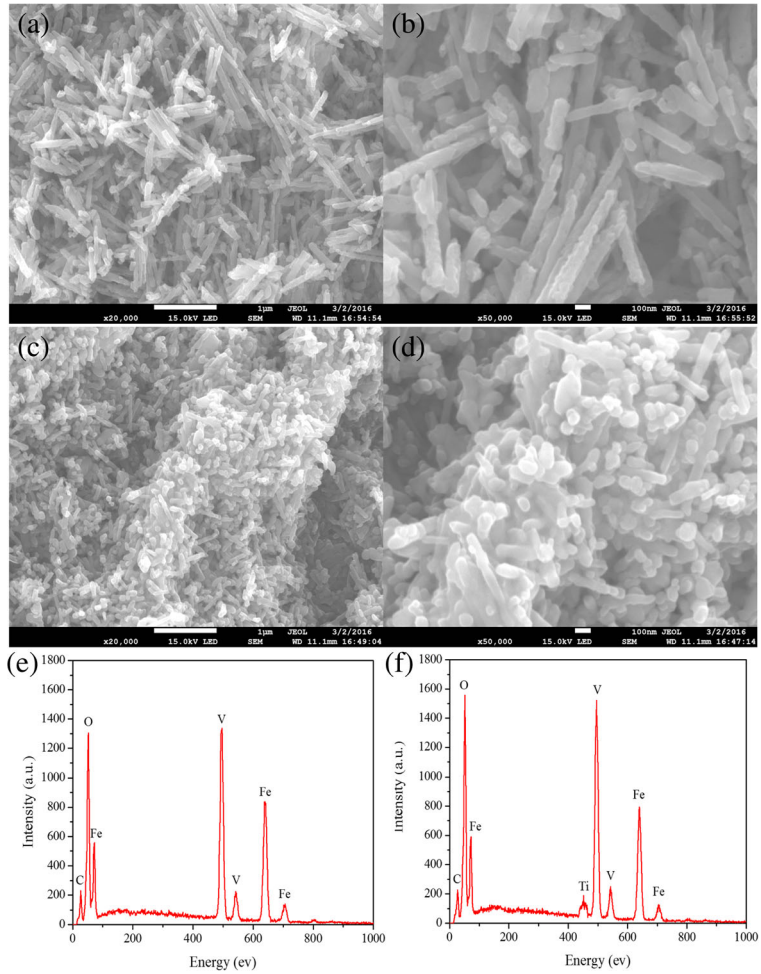

Fig. 3 SEM images of the samples: **a**, **b** $FeVO_4$; **c**, **d** $FeVO_4$@TiO_2. EDX spectra of **g** $FeVO_4$ and **f** $FeVO_4$@TiO_2

the $FeVO_4$@TiO_2 sample, which might be due to the low content and amorphous state of TiO_2. However, compared with porous $FeVO_4$ nanorods, the main diffraction peaks of $FeVO_4$@TiO_2 were weak in Fig. 1b.

As shown in Fig. 2, the X-ray photoelectron spectroscopy measurements were used to confirm the oxidation states of Fe, V, O, and Ti in $FeVO_4$@TiO_2. The peaks located at 711.3 and 724.5 eV identified with the binding energy of Fe $2p_{3/2}$ and $2p_{1/2}$. The peaks appearing at 516.8, 524.6, and 529.8 eV are attributable to the binding energy of $V2p_{3/2}$, $V2p_{1/2}$, and O1s. The weaker peaks at 458.6 and 464.2 eV correspond to the binding energy of Ti $2p_{3/2}$ and $2p_{1/2}$ (Fig. 2d), meaning the presence of Ti^{4+} in TiO_2. The combined results demonstrated that the $FeVO_4$@TiO_2 composite was obtained.

The particle morphologies of the as-prepared $FeVO_4$ and $FeVO_4$@TiO_2 were examined by SEM and TEM. As shown in Fig. 3a and b, uniform $FeVO_4$ nanorods were successfully obtained. Figure 3c and d show that the $FeVO_4$@TiO_2 composites retain the nanorods' structure, which would not be destroyed by TiO_2 encapsulation and thermal treatment. The EDX analyses show that Fe, V, and O are presented in the $FeVO_4$ samples, as shown in Fig. 3g; the uniform elemental Ti was distributed on the surface of $FeVO_4$@TiO_2 which is shown in Fig. 3f and Ti atom content in the composite was about 5%. The TEM images of the as-prepared $FeVO_4$ and $FeVO_4$@TiO_2 are shown in Fig. 4; these nanorods have widths of 100 nm and lengths of 0.3–2.0 μm, respectively. From Fig. 4b, it clearly shows that $FeVO_4$ nanorods have a hollow cavity structure (diameters of 5–25 nm). Upon TiO_2 encapsulation and calcination at 450 °C, the surfaces of the $FeVO_4$ nanorods (Fig. 4c) become relatively smooth and the HRTEM image in Fig. 2f showed apparent lattice fringes. The HRTEM image taken from the edge of the $FeVO_4$@TiO_2 samples

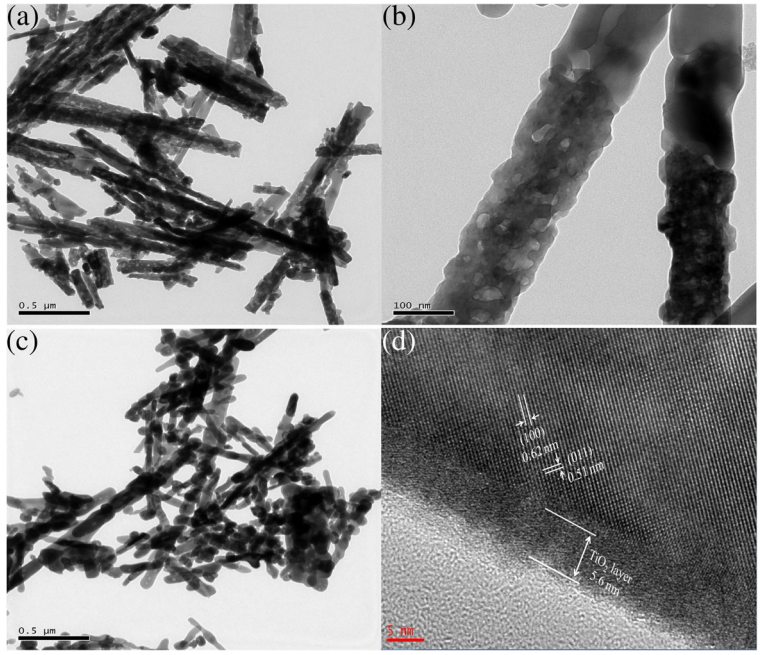

Fig. 4 **a**, **b** TEM images of the $FeVO_4$ samples. **c** TEM and **d** HRTEM images of $FeVO_4$@TiO_2 samples

showed the lattice fringe spacings of 0.62 and 0.51 nm (conforming to the interplanar spacings of the (100) and (011) lattice planes) of triclinic $FeVO_4$, respectively. A gray amorphous border is observed on the wall, which refers to TiO_2 layers (~5.6 nm).

Figure 5 presents the CV curves of the $FeVO_4$@TiO_2 samples. The CV curves were collected in a potential range of 0.01 to 3.0 V at a sweep rate of 0.3 mV s^{-1}. In the first curve, two reduction peaks at around 2.6–1.8 and 0.63 V, and the two obvious cathodic peaks observed at ~0.19 and ~0.46 V, can be assigned to the

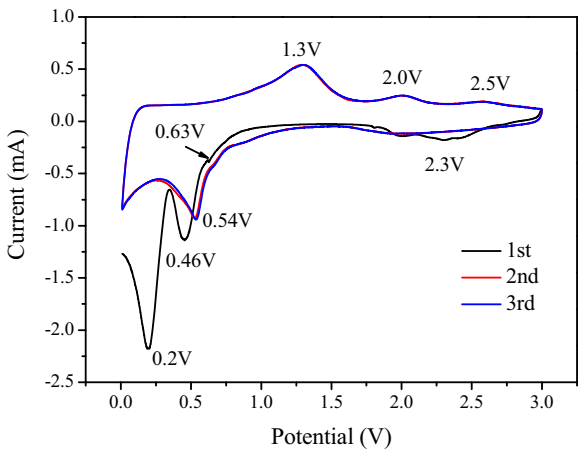

Fig. 5 First five cycles of CVs for the $FeVO_4$@TiO_2 electrode at a scan rate of 0.3 mV s^{-1} in the voltage range of 0.01–3.0 V

transformation of $FeVO_4$ into $Li_xV_2O_5$ and the reduction of Fe^{3+} to Fe^0, respectively. In this process, the electrochemical reactions can be described as: $xLi^+ + xe^- + FeVO_4 \rightarrow Fe + Li_xV_2O_5$ (Sim et al. 2012; Liu et al. 2017). From the following cycle, the peak of ~0.19 V disappeared, which implied an irreversible reaction occurring in this potential. The observation of phase transition of $FeVO_4$ in cycling is similar to that reported in literature (Ma et al. 2015; Ni et al. 2015). Due to the generated SEI layer and dissolution of the electrolyte solvent between the electrolyte and electrode, the electrode materials presented irreversible performance in the first cycle. The reduction peak at 0.46 V shifted to a positive direction at 0.54 V. The two obvious oxidation peaks at 1.3 and 2.04 V, a weak oxidation peak at ~2.5 V, are not changed from the initial cycle. Additionally, peaks at 1.7 V, which are attributed to the reduction peaks of anatase TiO_2 (Chen et al. 2015), suggest that the TiO_2 coating is active for lithium-ion intercalation. Except for the first cycle, the followed curves are nearly overlapped, indicating good reversibility for lithium ions to be intercalated and deintercalated in the $FeVO_4$@TiO_2 samples.

The electrochemical performances of $FeVO_4$ and $FeVO_4$@TiO_2 have been evaluated utilizing the coin-type cell. The cycling performance of the $FeVO_4$ and $FeVO_4$@TiO_2 electrodes for 100 cycles at 200 mA g^{-1} in the range from 0.01 to 3.0 V (vs. Li/Li^+) is shown in Fig.

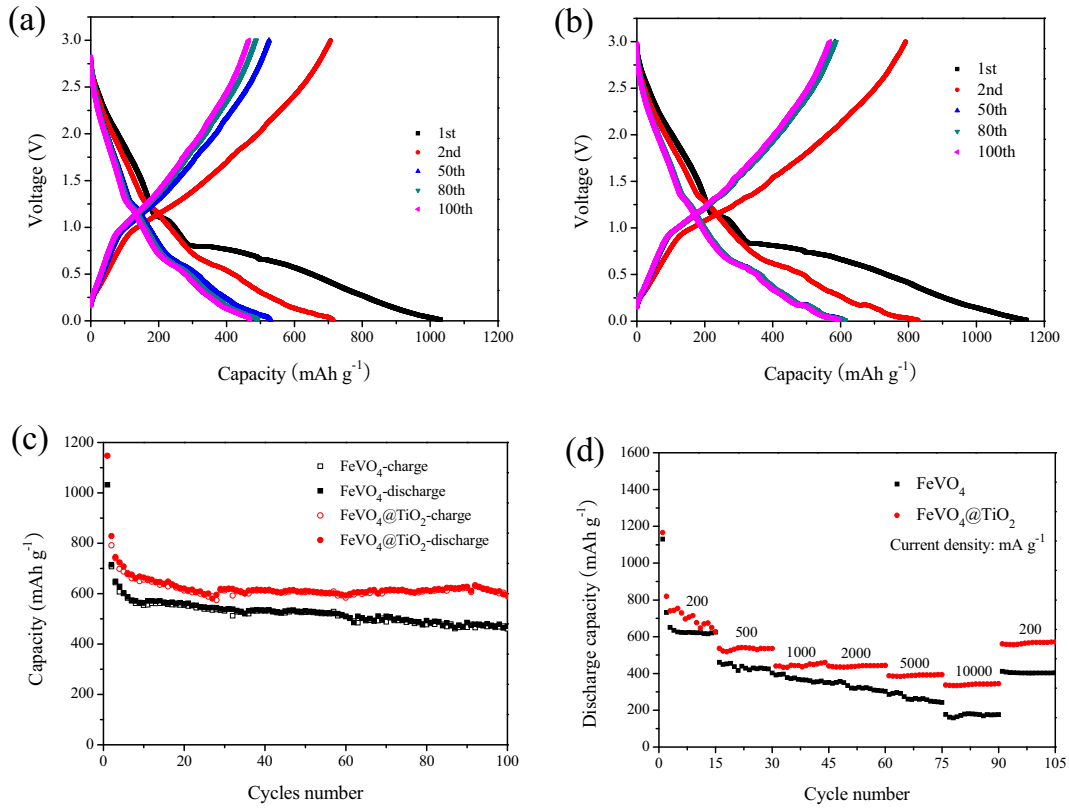

Fig. 6 Typical discharge/charge curves of **a** $FeVO_4$ and **b** $FeVO_4$@TiO_2; **c** cycling performance of the $FeVO_4$ and $FeVO_4$@TiO_2 electrodes; **d** cycling performance of the $FeVO_4$ and $FeVO_4$@TiO_2 electrodes at various current densities

6. The first discharge capacities of $FeVO_4$ and $FeVO_4$@TiO_2 were 1032 and 1147 mAh g^{-1}, respectively. The initial charge specific capacities of the $FeVO_4$ and $FeVO_4$@TiO_2 electrodes were 714 and 829 mAh g^{-1}; the first coulombic efficiencies were 69.2 and 72.3%, respectively. The cycle performance in Fig. 6c shows that $FeVO_4$@TiO_2 retains a capacity of 597 mA g^{-1} after 100 cycles. In contrast, the discharge capacity of $FeVO_4$ decreased to 470 mA g^{-1} at the same cycles. It is apparent that $FeVO_4$@TiO_2 has a better cyclic stability than $FeVO_4$. The highly stable amorphous TiO_2 provides protection for $FeVO_4$ from structural destruction through the charge/discharge processes.

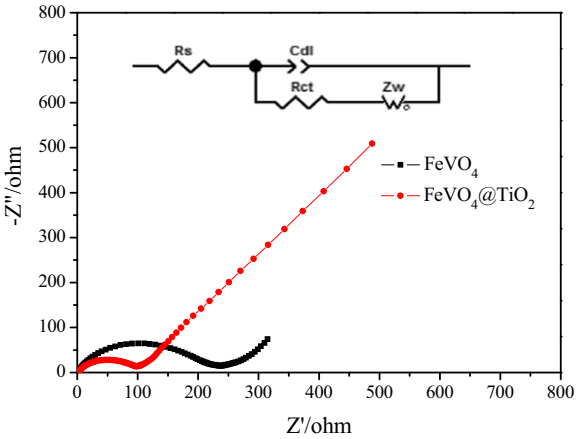

Fig. 7 Electrochemical impedance spectra (EIS) of **a** $FeVO_4$ and **b** $FeVO_4$@TiO_2. *Inset* The equivalent circuit used to interpret the spectra

In addition, the rate performance of the $FeVO_4$ and $FeVO_4$@TiO_2 is shown in Fig. 6d, in which the current density varied from 200 to 10,000 mA g^{-1}. The discharge capacities were obtained as 819, 536, 439, 436, 387, and 337 mAh g^{-1}, respectively, at discharge current densities of 200, 500, 1000, 2000, 5000, and 10,000 mA g^{-1}. The capacity was increased to 562 mAh g^{-1} when the current density was reverted to 100 mA g^{-1}, these results further implied that the $FeVO_4$@TiO_2 electrode behaved at a better cycle and rate performance than the bare $FeVO_4$ electrode (especially, 285 and 176 mAh g^{-1} at high current densities of

2000 and 5000 mA g^{-1}). The better rate capability of the $FeVO_4$@TiO_2 electrode can be ascribed to the coating of TiO_2 on the surface of $FeVO_4$.

To reveal the superior electrochemical performance of $FeVO_4$@TiO_2 compared with $FeVO_4$ for lithium energy storage, the charge-transfer resistance was tested by EIS over the frequency domain from 0.01 Hz to 100 kHz (Fig. 7). The result showed that the resistance of the $FeVO_4$@TiO_2 electrode was 97 Ω, which is lower than that of pure $FeVO_4$ (236 Ω). So, $FeVO_4$@TiO_2 shows better conductivity than $FeVO_4$, that is, the $FeVO_4$@TiO_2 electrode has accommodated the high current density during the cycles. It is why FeVO4@TiO_2 has a better cycling stability than $FeVO_4$.

Conclusions

In summary, a facile route to prepare porous $FeVO_4$ nanorods without any additives and template under hydrothermal conditions followed by calcinations was reported. To improve structural stability and cycle life, TiO_2 is used to coat the porous $FeVO_4$ nanorods. The $FeVO_4$@TiO_2 delivered a specific capacity of 1147 mAh g^{-1} at 200 mA g^{-1}. The discharge capacity remained at 596 mAh g^{-1} after 100 cycles, higher than that of pure $FeVO_4$. Compared with pure $FeVO_4$, $FeVO_4$@TiO_2 showed better electrochemical performances. The amorphous TiO_2 coating layer on $FeVO_4$ efficiently enhanced stability during the charging and discharging process, and this interesting synthesis method can also be applied to synthesize other materials with typical morphologies and properties.

Acknowledgments This work was financially supported by the Natural Science Foundation of China (No. 21476063) and is gratefully acknowledged.

Compliance with ethical standards

Conflict of interest The authors declare that they have no conflict of interest.

References

Chen XQ, Lin HB, Zheng XW, Cai X, Xia P, Zhu YM, Li XP, Li WS (2015) Fabrication of core–shell porous nanocubic Mn_2O_3@TiO_2 as a high-performance anode for lithium ion batteries. J Mater Chem A 3:18198–18206. doi:10.1039/C5TA04238K

Cheng FY, Chen J (2011) Transition metal vanadium oxides and vanadate materials for lithium batteries. J Mater Chem 21: 9841–9848. doi:10.1039/C0JM04239K

Gan LH, Deng DR, Zhang YJ, Li G, Wang XY, Jiang L, Wang CR (2014) $Zn_3V_2O_8$ hexagon nanosheets: a high-performance anode material for lithium-ion batteries. J Mater Chem A 2: 2461–2466. doi:10.1039/C3TA14242F

Huang WD, Gao SK, Ding XK (2010) Crystalline MnV_2O_6 nanobelts: synthesis and electrochemical properties. J Alloys Compd 495:185–188. doi:10.1016/j.jallcom.2010.01.116

Lei SJ, Tang KB, Jin Y, Chen CH (2007) Preparation of aligned MnV_2O_6 nanorods and their anodic performance for lithium secondary battery use. Nanotechnology 18:175605. doi:10.1088/0957-4484/18/17/175605

Li D, Duan XC, Qin Q (2013) Facile synthesis of novel α-Ag_3VO_4 nanostructures with enhanced photocatalytic activity. CrystEngComm 15:8933–8936. doi:10.1039/C3CE41365A

Liang LY, Xu Y, Wang X, Wang CL, Zhou M, Fu Q, Wu MH, Lei Y (2015) Intertwined $Cu_3V_2O_7(OH)_2{\cdot}2H_2O$ nanowires/carbon fibers composite: a new anode with high rate capability for sodium-ion batteries. J Power Sources 294:193–200. doi:10.1016/j.jpowsour.2015.06.076

Liu XL, Cao YC, Zheng H, Chen X, Feng CQ (2017) Synthesis and modification of $FeVO_4$ as novel anode for lithium-ion batteries. Appl Surf Sci 394:183–189. doi:10.1016/j.apsusc.2016.09.133

Ma H, Yang XJ, Tao ZL, Liang J, Chen J (2011) Controllable synthesis and characterization of porous $FeVO_4$ nanorods and nanoparticles. CrystEngCommun 13:897–901. doi:10.1039/C0CE00273A

Ma JJ, Ni SB, Zhang JC, Yang XL, Zhang LL (2015) The charge/discharge mechanism and electrochemical performance of CuV_2O_6 as a new anode material for Li-ion batteries. Phys Chem Chem Phys 17:21442–21447. doi:10.1039/C5CP03435C

Ni SB, Lv XH, Ma JJ, Yang XL, Zhang LL (2014) Electrochemical characteristics of lithium vanadate, Li_3VO_4 as a new sort of anode material for Li-ion batteries. J Power Sources 248:122–129. doi:10.1016/j.jpowsour.2013.09.050

Ni SB, Ma JJ, Zhang JC, Yang XL, Zhang LL (2015) Electrochemical performance of cobalt vanadium oxide/natural graphite as anode for lithium ion batteries. J Power Sources 282:65–69. doi:10.1016/j.jpowsour.2015.01.187

Pan AQ, Zhang JG, Cao GZ, Liang SQ, Liu J (2011) Nanosheet-structured LiV_3O_8 with high capacity and excellent stability for high energy lithium batteries. J Mater Chem 21:10077–10084. doi:10.1039/C1JM10976F

Peng B, Fan ZC, Qiu XM (2005) A novel transparent vanadate glass for use in fiber optics. Adv Mater 17:857–859. doi:10.1002/adma.200401271

Shi R, Wang YJ, Zhou F, Zhu YF (2011) $Zn_3V_2O_7(OH)_2(H_2O)_2$ and $Zn_3V_2O_8$ nanostructures: controlled fabrication and photocatalytic performance. J Mater Chem 21:6313–6320. doi:10.1039/C0JM04451B

Sim DH, Rui XH, Chen J, Tan HT, Lim TM, Yazami R, Hng HH, Yan QY (2012) Direct growth of $FeVO_4$ nanosheet arrays on stainless steel foil as high-performance binder-free Li ion battery anode. RSC Adv 2:3630–3633. doi:10.1039/C2RA20058A

Sun XJ, Wang JW, Xing Y, Zhao Y, Liu XC, Liu B, Hou SY (2011) Surfactant-assisted hydrothermal synthesis and electrochemical properties of nanoplate-assembled 3D flower-like $Cu_3V_2O_7(OH)_2{\cdot}2H_2O$ microstructures. CrystEngCommun 13:367–370. doi:10.1039/C0CE00083C

Sun Y, Hu X, Luo W, Xia FF, Huang YH (2013) Reconstruction of conformal nanoscale MnO on graphene as a high-capacity and long-life anode material for lithium ion batteries. Adv Funct Mater 23:2436–2444. doi:10.1002/adfm.201202623

Wang Y, Cao GZ (2008) Developments in nanostructured cathode materials for high-performance lithium-ion batteries. Adv Mater 20:2251–2269. doi:10.1002/adma.200702242

Wang M, Shi YJ, Jiang GQ (2012) 3D hierarchical $Zn_3(OH)_2V_2O_7{\cdot}2H_2O$ and $Zn_3(VO_4)_2$ microspheres: synthesis, characterization and photoluminescence. Mater Res Bull 47: 18–23. doi:10.1016/j.materresbull.2011.10.020

Wang JX, Yang X, Chen J (2014) Photocatalytic activity of novel $Ag_4V_2O_7$ photocatalyst under visible light irradiation. J Am Ceram Soc 97:267–274. doi:10.1111/jace.12639

Wu FF, Xiong SL, Qian YT, Yu SH (2015) Hydrothermal synthesis of unique hollow hexagonal prismatic pencils of $Co_3V_2O_8{\cdot}n\,H_2O$: a new anode material for lithium-ion batteries. Angew Chem Int Ed 54:10787–10791. doi:10.1002/anie.201503487

Xi GC, Ye JH (2010) Synthesis of bismuth vanadate nanoplates with exposed {001} facets and enhanced visible-light photocatalytic properties. Chem Commun 46:1893–1895. doi:10.1039/B923435G

Xiao LF, Zhao YQ, Yin J (2009) Clewlike ZnV_2O_4 hollow spheres: nonaqueous sol–gel synthesis, formation mechanism, and lithium storage properties. Chem Eur J 15:9442–9450. doi:10.1002/chem.200901328

Yan N, Xu Y, Li HJ, Chen W (2016) The preparation of $FeVO_4$ as a new sort of anode material for lithium ion batteries. Mater Lett 165:223–226. doi:10.1016/j.matlet.2015.11.061

Yang GZ, Cui H, Yang GW, Wang CX (2014) Self-assembly of $Co_3V_2O_8$ multilayered nanosheets: controllable synthesis, excellent li-storage properties, and investigation of electrochemical mechanism. ACS Nano 8(5):4474–4487. doi:10.1021/nn406449u

Yang GZ, Wu MM, Wang CX (2016) Ultrathin $Zn_2(OH)_3VO_3$ nanosheets: first synthesis, excellent lithium-storage properties, and investigation of electrochemical mechanism. ACS Appl Mater Interfaces 8(36):23746–23754. doi:10.1021/acsami.6b08048

Yin ZG, Xiao Y, Wang X, Wang W, Zhao D, Cao MH (2016) MoV_2O_8 nanostructures: controlled synthesis and lithium storage mechanism. Nano 8:508–516. doi:10.1039/C5NR05602K

Zhang SY, An W, Wu G (2015) $Cu_5(VO_4)_2(OH)_4{\cdot}H_2O$ nanobelts as anode materials for lithium-ion batteries. Chem Phys Lett 621:1–4. doi:10.1016/j.cplett.2014.12.047

Zhu Q, Wang WS, Lin L (2013) Facile synthesis of the novel Ag_3VO_4/AgBr/Ag plasmonic photocatalyst with enhanced photocatalytic activity and stability. J Physical Chemistry C 117:5894–5900. doi:10.1021/jp400842r